

SCIENTIFIC REPORTS

OPEN

Lithosphere strain rate and stress field orientations near the Alpine arc in Switzerland

N. Houlié^{1,2}, J. Woessner^{3,4}, D. Giardini¹ & M. Rothacher²

In this study we test whether principal components of the strain rate and stress tensors align within Switzerland. We find that 1) Helvetic Nappes line (HNL) is the relevant tectonic boundary to define different domains of crustal stress/surface strain rates orientations and 2) orientations of *T*-axes (of moment tensor solutions) and long-term asthenosphere cumulative finite strain (from SKS shear wave splitting) are consistent at the scale of the Alpine arc in Switzerland. At a more local scale, we find that seismic activity and surface deformation are in agreement but in three regions (Basel, Swiss Jura and Ticino); possibly because of the low levels of deformation and/or seismicity. In the Basel area, deep seismicity exists while surface deformation is absent. In the Ticino and the Swiss Jura, where seismic activity is close to absent, surface deformation is detected at a level of $\sim 2 \cdot 10^{-8}$ /yr ($\sim 6.3 \cdot 10^{-16}$ /s).

Motivation. GPS networks, that measure long-term deformation at the surface, provide a unique opportunity to place seismic activity in context with geological observations resulting of long periods of tectonic activity (i.e. sea-level changes, geology, and erosion rates). Although they highlight various periods of times, the relationship between surface deformation (i.e. GPS), crustal seismicity (i.e. moment tensors principal components), and strain in the asthenosphere (i.e. shear wave splittings) is of genuine interest, both for understanding the origin of the surface deformation observed and quantifying seismic hazard. For instance, the comparison of directions of principal components of both stress and strain tensors helps understanding whether stress accumulates along faults^{1–5} or through blocks^{6–8}, whether seismic ruptures are triggered^{9–15}, encouraged or impeded¹⁶ and, finally, how stress is transferred to surrounding fault systems^{17–20}. Also, the comparison between strain rates and asthenosphere strains sheds light on the upper mantle strength^{21,22} and reveals whether the current tectonic period could be responsible and/or parented to the anisotropy detected in the mantle^{23–25}.

Across strongly active plate boundaries, linking seismic activity and surface deformation is made easier because strain rates are high ($> 10^{-7}$ /yr) and permanent GPS networks are dense^{26–28}. There, higher strain rates tend to shorten seismic cycles lengths²⁷, enabling us to document larger portions of the seismic cycle and informing us on the preparation of future mainshocks. For slowly deforming intra-plate regions, however, we understand less about the relationship between surface deformation and seismicity: strain rates are smaller, seismic activity may not be sufficient to deform the surface while seismic hazard may still be significant^{29–32}. We take Switzerland for an example of this situation and investigate the link between GPS strain rates and the seismicity observed since 2 decades.

Seismic Activity. At the meeting point between the central European platform and the Adria plate (Fig. 1a), Switzerland is at a key location to understand the dynamics of lithosphere in the region. Over the last millennium, historical earthquakes such as for $M_w = 6.6$ Basel 1356^{33–36}, $M_w = 6.2$ Churwalden 1295^{37,38}, $M_w = 6.1$ Visp 1855 Valais^{39–44} and $M_w = 6.1$ Sierre 1946^{45,46} were reported. Since 1500's six $M_w \sim 6.0$ events in the wider Valais area⁴⁷ ruptured different fault systems with an average recurrence interval of ~ 100 years⁴⁸. Another peculiarity of Switzerland's seismicity lies in its depth distribution (Fig. 2a). North of the Helvetic Nappes (HN), hypocentre depths are limited to the upper crust with extreme values up to Moho depths (~ 35 km) near Luzern, while south of the HN, the earthquakes depths remain shallower than 15 km^{49,50}. The transition from shallow to deep seismicity was interpreted as an indication of high pressure fluids⁵¹. Such a transition (topography, geology) between the Swiss Molasses and the Alpine arc domain cannot be confirmed using the moment tensor catalogue: most

¹ETH-Zurich, SEG, Sonneggstrasse 5, 8092, Zürich, Switzerland. ²ETH-Zurich, MPG, HPV G 53, Robert-Gnehm-Weg 15, 8093, Zürich, Switzerland. ³ETH-Zurich, SED, Sonneggstrasse 5, 8092, Zürich, Switzerland. ⁴Present address: Risk Management Solutions (RMS), Stampfenbachstrasse 85, CH-8006, Zurich, Switzerland. Correspondence and requests for materials should be addressed to N.H. (email: nhoulie@alumni.ethz.ch)

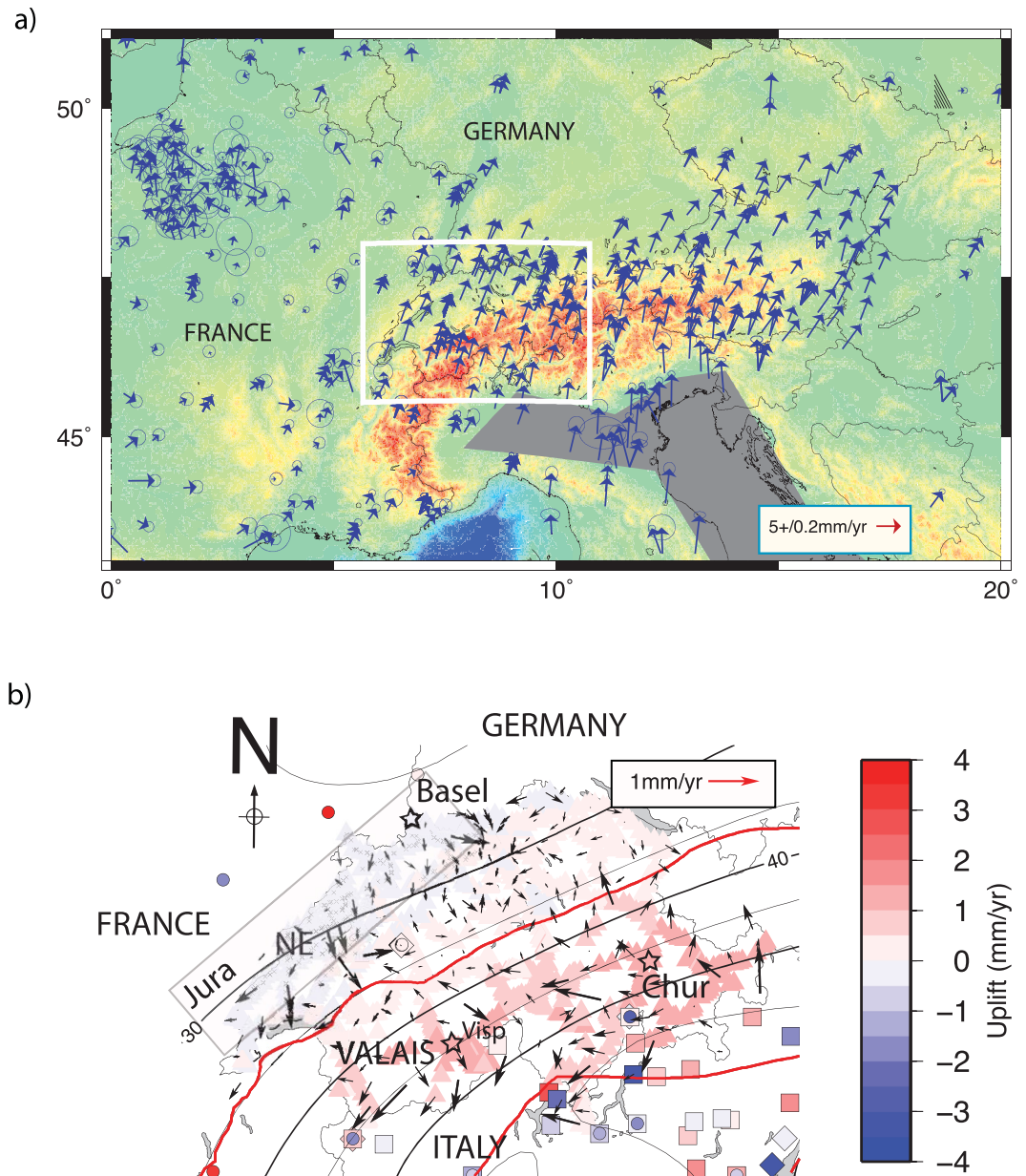


Figure 1. (a) Regional GPS velocity field (blue, stable Eurasia fixed) in western and central Europe in the vicinity of the Alpine arc and of the Adria plate. (b) Comparison of relative GPS horizontal velocities (black arrows), SWISSTOPO levelling (triangles) vertical rates⁷⁰ and GPS vertical rates^{74,96} (squares and diamonds correspond to Serpelloni *et al.*, 2013 and Cenni *et al.*, 2013's measurements, respectively). Levelling rates and GPS vertical rates in Italy are indicated with color-coded triangles and color-coded squares. All geodetic motions are plotted with respect to the site ZIMM (circle inside a square). Moho depths (km)^{97,98} are overlaid using black lines (one line per 5 km). A reasonable correlation between Moho depth and highest uplift rates (>1 mm/yr) is visible. NE stands for Neuchatel. HNL and Insubric lines are indicated in red and green, respectively. This figure has been created using Generic Mapping Tools 4/5⁹⁹ and Adobe Illustrator CS3.

focal mechanisms (first motions solutions) are of strike-slip type except in the southern Valais (Fig. 2b). This last observation raises questions regarding the tectonic status (active, non-active) and real nature of the Alpine arc's current dynamics (e.g. resulting of gravitational spreading, surface expression of a lithosphere discontinuity).

Surface Deformation. The surface deformation of the region is limited^{52–54}, and is considered to be in agreement with moderate-to-low level of seismic activity. Horizontal strain rates ($<10^{-7}$ /yr) are likely the consequence of the motion of the Adria plate^{55,56} towards the North-East^{57,58}. Because of current shortening rates are small (<3 mm/yr⁵⁹) and knowing the total convergence is from 300⁶⁰ to 480 km⁶¹, the Alpine belt is today seen either as inactive^{62,63} and/or close to isostatic equilibrium⁶⁴. The latter is in agreement with vertical rates (up to 1.2 mm/yr south of the Helvetic Nappes) observed by both multi-decadal levelling^{65,66} and GPS measurement

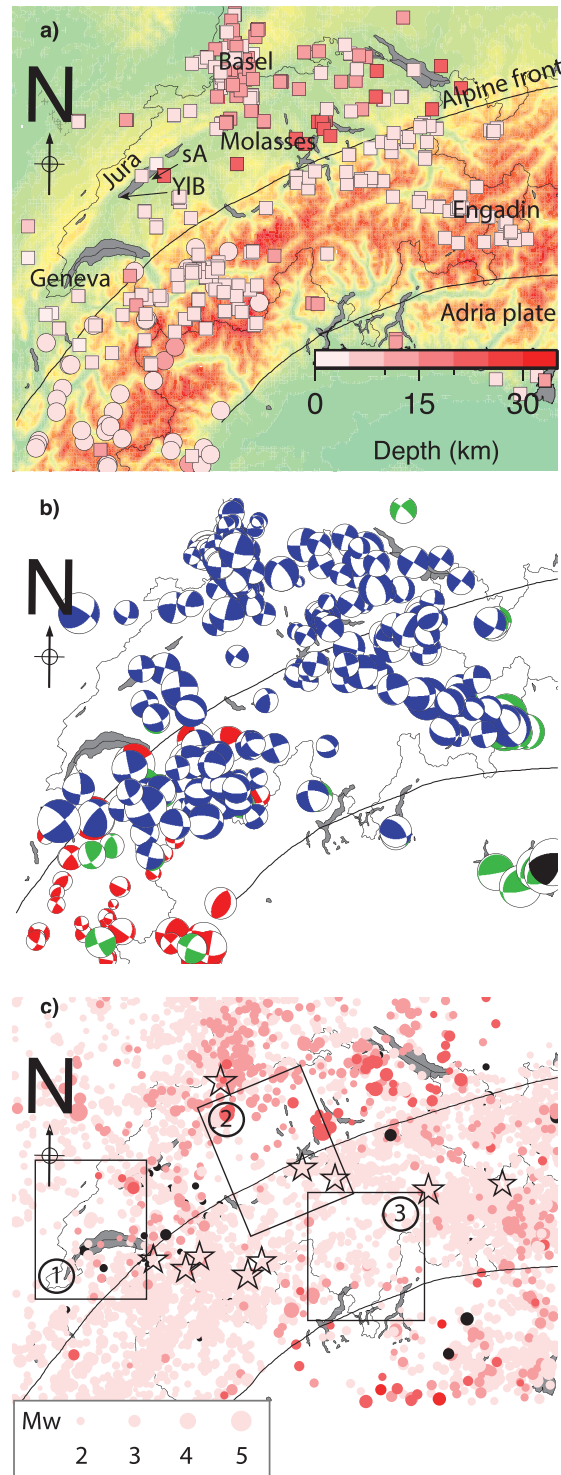


Figure 2. Seismicity characteristics. (a) Depth of earthquakes hypocenters. If we exclude the Geneva area, largest earthquakes are deeper north of the HNL (>12 km). The transition between deeper and shallower seismicity is visible across the HNL where the uplift rates are the highest. sA and YIB stand for St-Aubin and Yverdon-les-bains. (b) First-motion focal mechanisms^{49,81,94,100,101}. [Green: International Seismological Center (ISC); Red: Sue and Delacou *et al.*, 2004; Blue: Kastrop *et al.*, 2004 + Deichmann *et al.*, 2012 + Marschall *et al.*, 2013; Black: QRCMT INGV]. Most events mechanisms are close strike-slip type suggesting that the orientations of principal stress axes are located in the horizontal plane (σ_3 nearly vertical). Helvetic Nappes (HN) and Adria plate boundaries are drawn (black lines¹⁰²). (c) ECOS-09 seismicity catalogue³⁷. This figure has been created using Generic Mapping Tools 4/5⁹⁹ and Adobe Illustrator CS3.

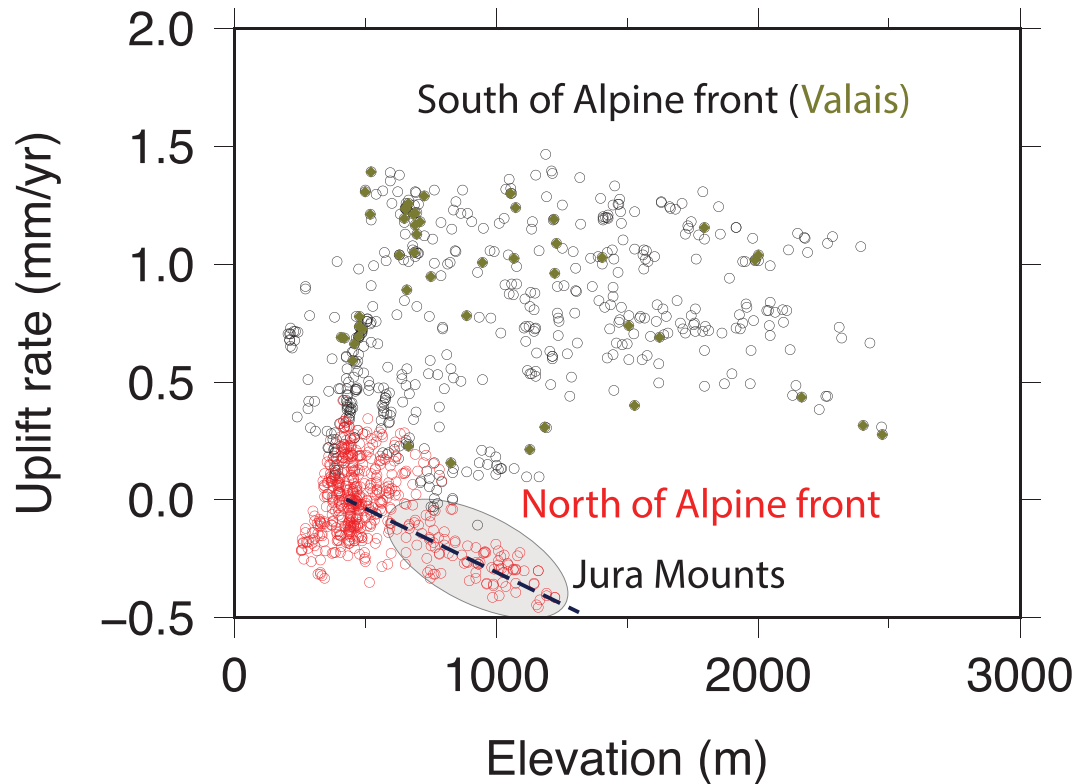


Figure 3. Uplift rates obtained from repeated levelling campaigns as a function of the elevation. No correlation is found between rates and elevations except in the Jura (grey ellipse) where highest points are also the fastest subsiding ones. Levelling vertical rates⁷⁰, and topography from SWISSTOPO (200 m resolution). This figure has been created using Generic Mapping Tools 4/5⁹⁹ and Adobe Illustrator CS3.

campaigns^{67–70}. Because uplift rates are densely mapped in Switzerland, such a whole-arc view on vertical motions can however be refined. For instance, there is no correlation between elevation of the topography and uplift rates inferred of levelling campaigns, except in the Jura arc (Fig. 3). There, the uplift rates are in agreement with levelling measurements made in the Rhine graben⁷¹ or in the Jura very locally⁷², but are also anti-correlated with elevations in Jura at the arc scale (Fig. 3). On the horizontal plan, the situation is also complex, reflecting the interplay between inherited geology⁷³ and active processes. Together, horizontal convergence and uplift variations⁷⁴ explain why, even if they remain rare, large magnitude ($M_w > 6.0$) earthquakes occur³⁷.

In order to understand the tectonics acting in the central Alps in Switzerland, we 1) map the strain rate field measured using GPS during the last 2 decades, 2) investigate whether the *HN* can be associated with changes of orientations of the principal components of the strain tensors and 3) at last, by comparing those with orientations of *P*/*T*- axes, and fast axes of shear waves splittings, we discuss whether the orientations of principal components of the stress tensors constrained by moderate magnitude seismic events ($M_1 > 2.0$) are compatible with mantle deformation observed in the region⁶³.

Results

At the country scale, shear and extension rates dominate compression rates (Fig. 4a–d). This observation fits well with a crustal seismicity mostly composed of strike-slip events and with previous studies focusing on long-term deformation of central and western Alps^{75,76}. Spatially, the *HN* cannot be seen as a limit across which strain rates vary. Indeed, in the region of Lausanne and Geneva (shear rates up to $\sim 4.0 \cdot 10^{-8}$ strain/yr, Fig. 4c) and within in the Jura arc ($\sim 2.0 \cdot 10^{-8}$ strain/yr), deformation is detected. Unlike seismicity (Fig. 4c), strain rates are spatially homogeneous. However, such a crude view of Switzerland's surface deformation is quickly challenged by comparisons of seismicity and strain rates performed at a more local scale.

In specific areas, we find apparent discrepancies between strain rates and seismic activity (i.e. occurrence of earthquake).

- In the central Jura, \sim NW-SE extension is found (Fig. 4a) while only low seismicity is observed. This observation appears to be surprising although it is not the first time that extension was constrained across the Jura arc: the same conclusion was reached after mapping the strain field of Switzerland using 3D interpolation of strain rates on a regular grid⁷⁷; and after a joint processing of the AGNES/COGEAR datasets⁷⁸. The extension is therefore not due to an artefact of network geometry or an interpolation issue. Due to the poor density of the network in the region, extension across the Neuchâtel lake is not the unique mechanism that is able to explain the GPS vector field in this area. The same vector field could be generated by the motion associated

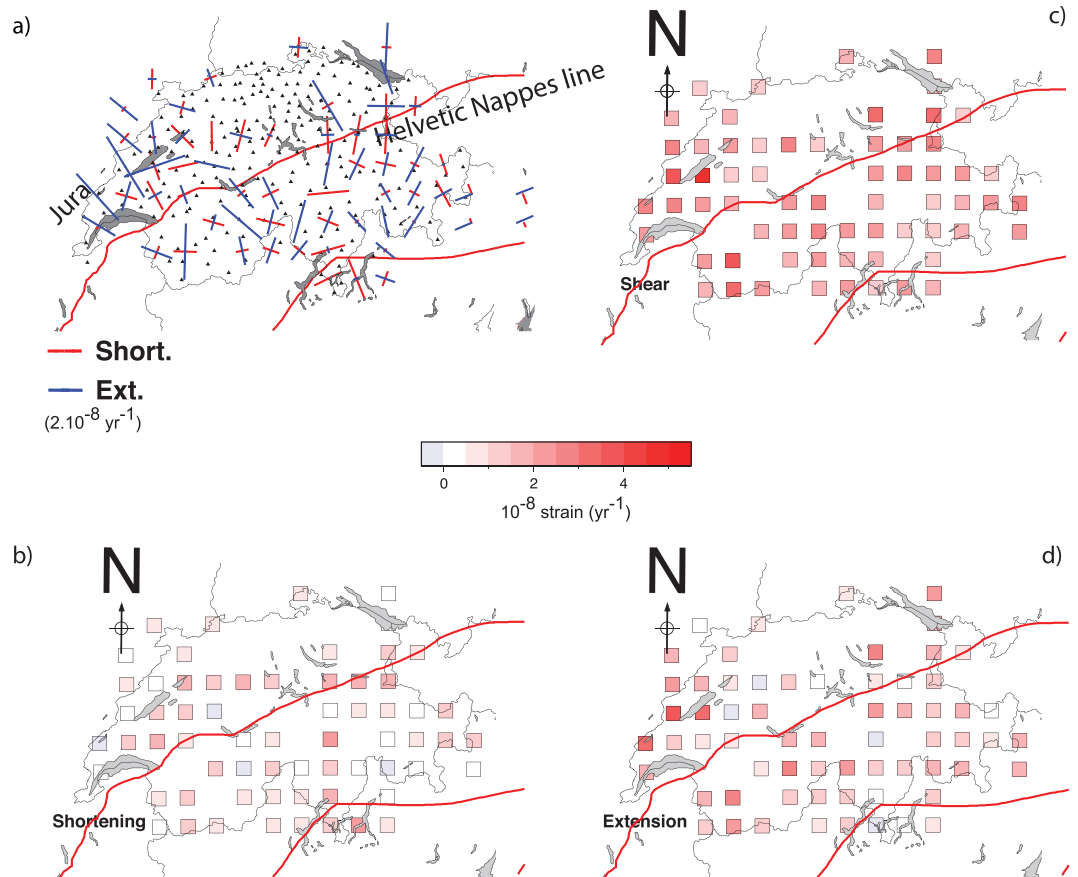


Figure 4. Horizontal strain field of the central Alps and Switzerland computed the inversion of GPS data. Alpine front and Adria plate are indicated using red lines. **(a)** Principal strain rate axis (compression in red, extension in blue) computed using the SSPX 2D algorithm⁹⁵. Strain rates have been estimated using a near-neighbour smoothing strategy (grid spacing 25 km, 6 neighbours, maximal distance = 50 km). Shear and extension dominate the strain field in the whole country. Some areas such as Luzern, Zurich and Basel remain un-deformed even if they are the places of active seismicity; **(b)** magnitude of maximum shortening rates **(c)** maximum shear strain rate and **(d)** Maximum extension rate. Basel (BA), Geneva, (GE), Luzern (LU), Konstanz (KS), Zurich (ZU), Valais (VA) and Ticino (TI) are indicated on panel b. Average shear, extension and shortening strain rates are respectively equal to $2.2 (\pm 0.8) 10^{-8}/\text{yr}$, $1.4 (\pm 0.10) 10^{-8}/\text{yr}$ and $-7.7 (\pm 0.6) 10^{-8}/\text{yr}$. This figure has been created using Generic Mapping Tools 4/5⁹⁹ and Adobe Illustrator CS3.

with a strike slip fault oriented NW-SE and located between the localities of St Aubin and Yverdon-les-bains. Such faults have been documented in the area⁷⁹, but further investigation will be necessary to identify which tectonic structure may be responsible for the deformation observed.

- South of the *HN*, directions of maximum shortening are parallel to the front, (i.e. ~E-W direction) except in the east near Engadin where shortening directions are ~N-S (Fig. 8b). This observation is well in agreement with observation made across the Italy-Switzerland border⁸⁰.
- In the north-western Valais, the ~N-S extension (few ~E-W compression) is in agreement with the focal mechanisms (Fig. 2b) inferred from first motion arrivals⁸¹.
- In the north-east of the Swiss Molasses, no substantial deformation is observed where diffuse seismicity is still observed (Fig. 2c). In the Ticino, both uplift (~1.0 mm/yr) and deformation ($2.0 10^{-8}/\text{yr}$) are observed while $M_w > 4$ earthquakes are absent in historical seismicity catalogues of this area³⁹. There, the GPS network is not dense enough to capture local deformation.

In a situation in which strain rate is detected but earthquake magnitudes are too small to complete a moment tensor analysis, we attempt to use the strain rate field to characterize the regional stress field through the orientation of principal stress component. Indeed, it has been shown²¹ that the directions of strain rate tensor components inferred from GPS are a good proxy of the principal stress components projected in the horizontal plane (i.e. ~orientation of S_H). Following the same idea, orientations of principal components of the strain rate tensor components with borehole breakouts orientations were successfully compared²². Here, we compare directions of the maximum shortening rates (GPS) with *P*-/*T*- axes orientations in order to constrain the orientation of σ_1 . Comparison of orientations of S_H and *P*- axes have been used in the past to infer the direction of σ_1 at the local scale^{82–84} within uncertainties⁸⁵. The alignment of maximum shortening directions with S_H and *P*- orientations would imply that the lithosphere strain rates and crustal stress fields are consistent. First, we find that strain and

	All CH	North of Alpine front	South of Alpine front	Reference
Shortening	81 +/- 49	65 +/- 49 (N=24)	97 +/- 38 (N=37)*	This study
Extension	-8 +/- 49	7 +/- 1 (N=12)	-5 +/- 49 (N=21)	This study
SKS	39 +/- 17	39 +/- 17 (N=8)	38 +/- 17 (N=14)	⁶³
P-Axes	151 +/- 38	158 +/- 32 (N=110)	143 +/- 43 (N=95)	⁹⁴
T-axes	41 +/- 32	54 +/- 31 (N=110)	26 +/- 25 (N=95)	⁹⁴
P-axes**	153 +/- 28	N/A	N/A	¹⁰⁴
T-axes**	66 +/- 18	N/A	N/A	¹⁰⁴

Table 1. Azimuths (deg. N) of T- and P- axes, directions of maximum shortening, extension and SH. *We excluded the 5 points located south of the Alpine front but deformed by principal strain shortening in the NS direction (circle on Fig. 8c). **Only events located within 12 km above the Moho are considered here.

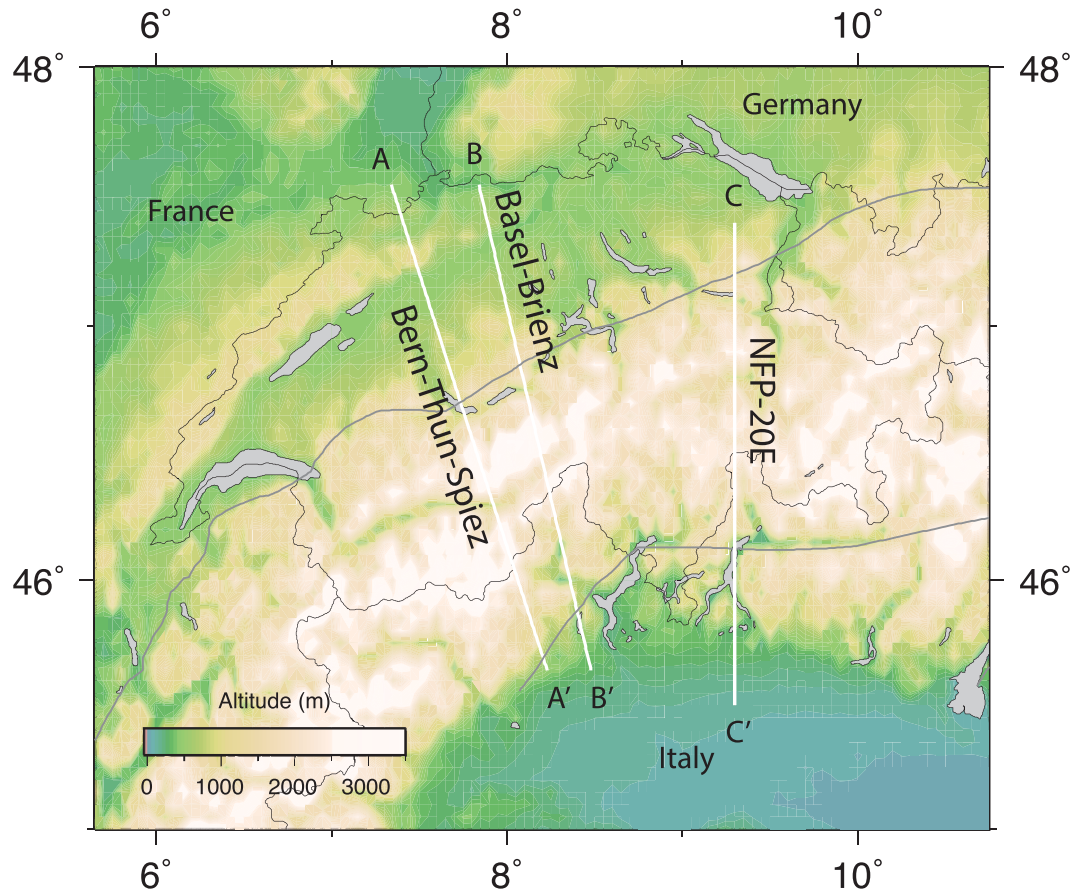


Figure 5. Map showing the locations of profile used in Figs 6 and 7. This figure has been created using Generic Mapping Tools 4/5⁹⁹ and Adobe Illustrator CS3.

stress components orientations are similarly scattered (~20 degrees; Table 1) both north and south of the HN. Interestingly, shortening strains, *T*- and *P*- axes orientations rotate across the HN of +32, -28 and -15 degrees N, respectively (Table 1). Rotation is well visible for the strain principal axes along defined profiles but also within groups (Figs 5, 6 and 7). Everywhere, the orientations of maximum shortening and of *P*- axes fall in the same quadrant (Fig. 8) and are associated with the location of HN (or to the Basal Alpine thrust). Such an agreement suggests that 1) south of the HN the maximum shortening axes directions can be considered a good proxy for the direction of the principal stress component and therefore 2) lithosphere deformation and crustal seismic activity are consistent. The spatial consistency of the rotation for strain/stress datasets, nevertheless of their inherent diversity and of their lack of causality (it is difficult to understand how one induces the other), implies that both strain-rate and stress fields are induced by a same set of forces deforming the crust and possibly the lithosphere at the regional scale. From this spatial analysis we conclude that the HN delimit spatially two regimes of deformation and seismic activity. Variation of the strain rates across the Alpine arc is not visible, suggesting the strain is well distributed across fault systems, as observed in the seismicity catalogue (Fig. 2c).

Regarding the balance between long- and short-term deformation, we complete a comparison between shear wave splittings (SKS phase) and surface deformation. As shown in New-Zealand²² and California 2012²¹, the

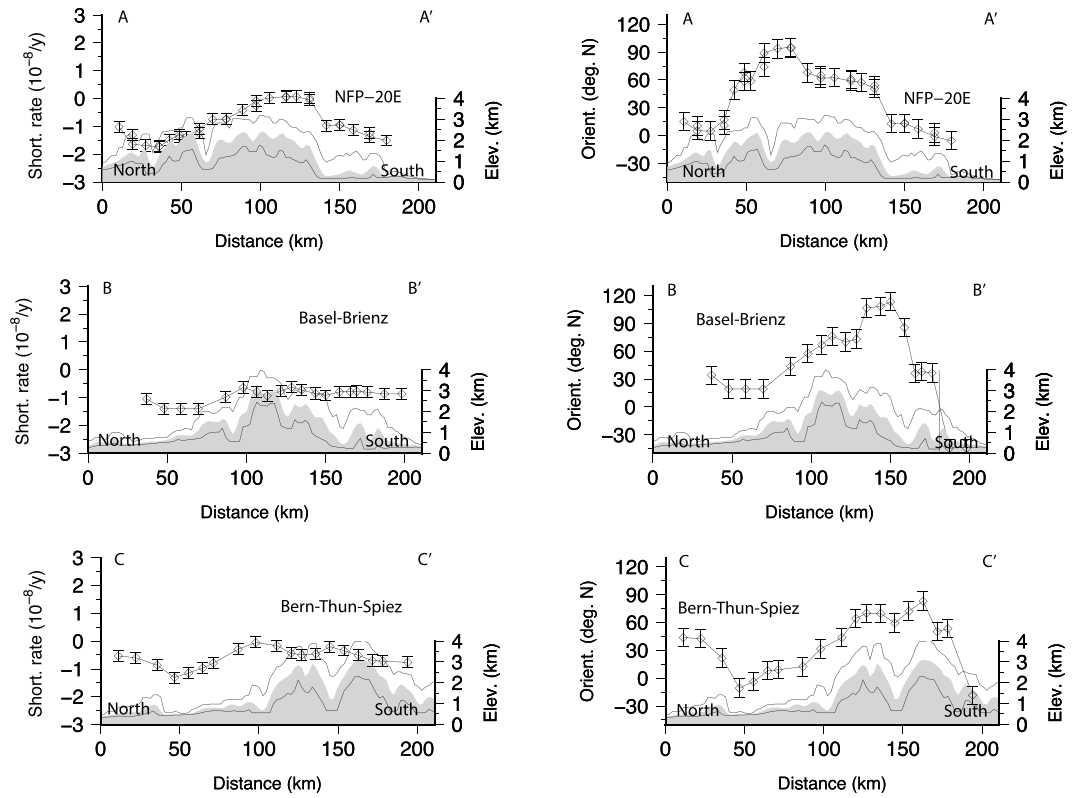


Figure 6. (a) Directions of maximum shortening as shown in Fig. 4b; (b) Maximum shortening rates along the profiles shown in Fig. 5. This figure has been created using Generic Mapping Tools 4/5⁹⁹ and Adobe Illustrator CS3.

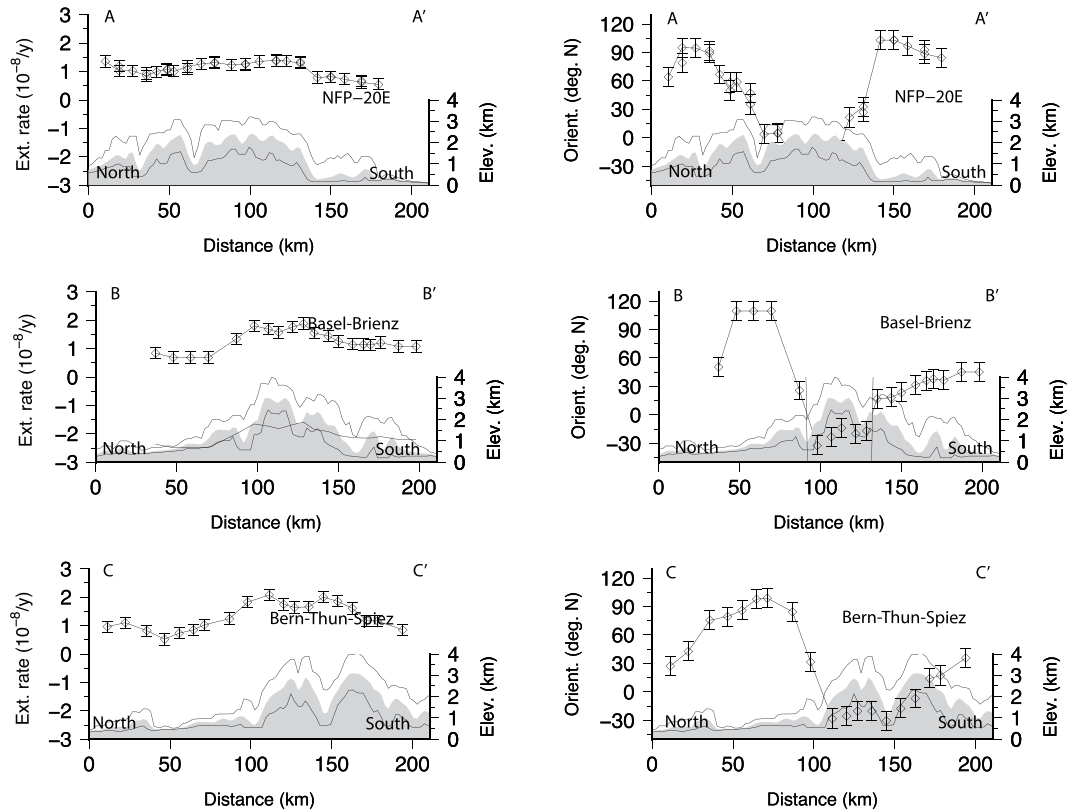


Figure 7. (a) Directions of maximum extension as shown in Fig. 4b; (b) Maximum extension rates along the profiles shown in Fig. 5.

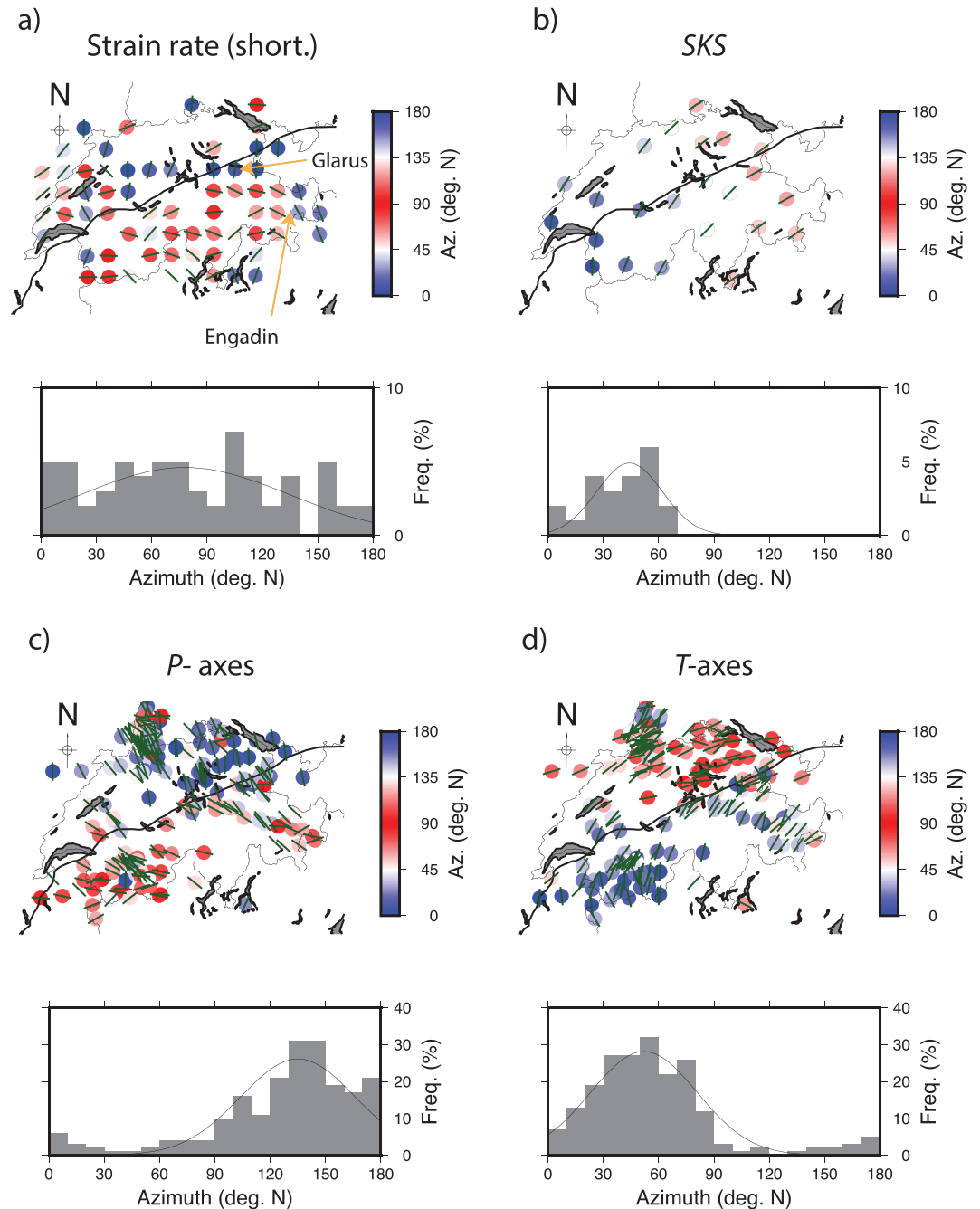


Figure 8. (a) Orientation of maximum shortening in Switzerland. South of the Alpine front shortening is oriented in the ~EW direction (N90) but cannot be determined in the Molasses, South of the Alpine front, in the Jura area, the picture remains more complex. The limits of the Alpine front is not sufficient to explain why in the east Engadin area the shortening orientations are 90 degrees (at ~N180) to the orientations observed anywhere else south of the Alpine front. (b) Fast axis of shear wave splitting⁶³. GPS shortening directions rotate across the Alpine front while fast axis of shear wave splittings not. Unlike the other datasets, the orientation of the fast axes of shear wave splittings do not rotate. In many places, the orientations of T- axes are sub-parallel to the fast axes of shear wave splittings. (c) Orientation of P-Axes in Switzerland, north and south of the Alpine front. A 30 degrees (anti-clockwise) rotation is observed across the Alpine front line. North of the Alpine front, P- axes are ~perpendicular to the Alpine front, in agreement with the orientation of the S_H in the Molasses¹⁰³. (d) Orientation of T-Axes in Switzerland. In most Switzerland, T-axis are sub-parallel to the Alpine front. For each panel, we show the statistical distribution of each dataset plotted in the 0–180 degrees range. Mean orientations for directions of maximum shortening, P-, T- axes and fast axes of shear wave splittings are ~N80, ~N140, ~N50 and N37 respectively.

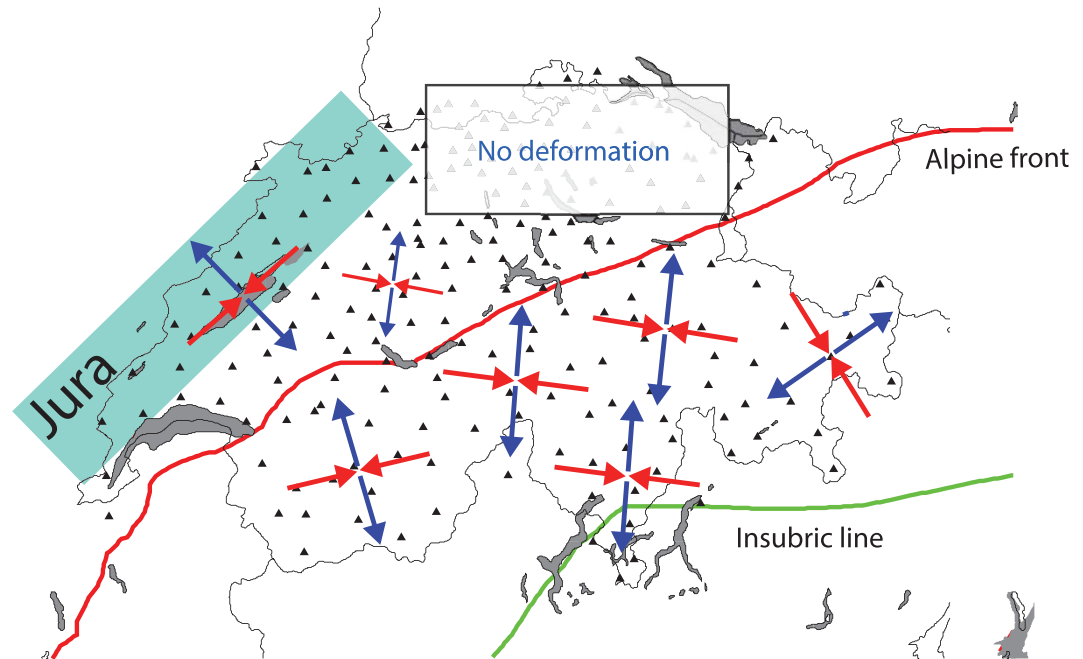


Figure 9. Summary sketch showing deformation in the study area.

comparison between surface deformation rate measured by continental (20–50 km spacing) GPS networks and shear-wave splittings measurements allows the comparison between current average lithosphere deformation and vertically cumulated strain as sampled by seismic waves (SKS and SKKS) through, asthenosphere and lithosphere. In western and central Alps, the presence of Lattice Preferred Orientations (LPO) anisotropy (delays δt up to ~ 2 s) has been detected⁶³. Amplitudes of travel time delays leave little doubt about their origin. Cumulating such large time delays over a wide region while keeping their orientation stable (only ± 17 degrees of variation within Switzerland) would require a strong organization of the deformation of crustal layers in all directions, which is not observed. We conclude then that the strain mapped using SKS splitting's originates mostly from mantle deformation and the contribution of crustal anisotropy must be limited. However, because of the inherent difficulty to date strain, it is not possible to determine whether the asthenosphere flow was still active and/or only recent using shear-wave splittings only⁶³. Here we have an opportunity to solve this problem by comparing fast axis of shear wave splitting with seismicity and strain/stress fields measured today. South of the HN, the shear-wave splitting directions (38 ± 17 degree north) are consistent with both the orientations of T -axes (26 ± 25 degree north) but less with directions of maximum extension (-5 ± 49 degree north). This suggests that 1) a significant amount of finite strain is present through the Alpine arc (they are ~ 40 degrees off to the GPS extension rates). North of the HN in the Neuchatel area, the directions of fast axes of shear wave splitting's align with directions of maximum shortening (Fig. 8a and b); implying either decoupling at the base of the lithosphere (or within the crust) exists or that the surface deformation observed is of shallow origin.

Conclusion

Switzerland represents a transition between stable continental regions with infrequent moderate to large magnitude events ($M_w < 6$) and more active areas where mainshocks ($M_w > 6$) occur every 50 years or less. We compare GPS surface strain rate field, shear wave splitting measurements, and principal components of crustal stress (P -/ T -axes) of Switzerland in order to get a clearer picture of the processes active today. Each dataset gives access to various time- (from 10^2 yr to $>10^5$ yr) and space-scales (from 10^4 m to 10^5 m) that we compare in the same framework.

At the country scale, seismicity and lithosphere strain rates are compatible through their respective orientations. We find the HN to be a major discontinuity that allows mapping both the changes of orientations of principal components of strain-rate and stress tensors and the changes in the seismicity depths (Fig. 9). The agreement of long- and short-space scale measurement seems to suggest that the central Alps are not close to experience a rapid extensional collapse such as described elsewhere^{86,87}. The Jura, however, seems to be the place of a current geologic activity (i.e. extension combined with subsidence) that will require more investigations to be better understood.

Strain accumulated in the Valais and the Ticino are of similar amplitudes ($\sim 2 \cdot 10^{-8}$ /yr), while the seismic moment released in the Ticino is ten times smaller than in the Valais and may therefore either 1) lead to an event of significant magnitude that is not present in today's historical catalogue for this area or 2) could be explained by the occurrence of dislocation creep within the lithosphere.

Albeit we suggest that strain rates constrained from surface measurements fit well with the orientations of the stress components in the crust during the period covered by seismicity catalogues, we stay aware that the current lithosphere seismic activity as we measure it today may be well not representative of longer periods of time; the

Network solutions	Campaigns / Stations	Date
LV95	24 campaigns, 287 points	1988–1995
LV95 densification	32 campaigns, 134 points	1995–1998
CHTRF98 + +	8 campaigns, 215 points	1998–2002
EUVN97	1 campaign, 217 points	1997
AGNES	4.5 years permanent observed, 85 points	1998–2003

Table 2. Description of the GPS campaigns¹⁰⁵ carried out by SWISSTOPO corresponding to vectors shown in Fig. 1b.

Catalogue	Number of events	Average seismic Moment (M_0 in 10^{12} /yr)	Period covered	Reference
First motions	141	0.36 +/- 1.12	1968–1999	¹⁰⁶
First motions	211	0.27 +/- 0.6	1968–2013	¹⁰⁷
Magnitude	9559	0.52 +/- 0.5	1991–2008	³⁷

Table 3. Seismicity catalogues used in this study. Seismic moment rates are shown in Fig. 9.

clustered seismicity observed in Switzerland could well suggest that even if slip rates are small today, they may vary over time periods as it has been observed in more active areas^{16,88,89}.

Materials and Methods

A-Datasets. We use two datasets that have their own spatial and temporal resolutions.

- First, we use a catalogue of moment tensor solutions (first motions) for Switzerland ($M_w < 5$) to inform us on the orientation of the stress field through the analysis of *P*- and *T*- axes orientations. Principal axes of the moment tensor solutions give approximate orientation of the local stress field in the crust and span over the last ~40 years.
- Second, we use the strain rates computed from GPS velocity fields. Because of the GPS network density (< 1 site per 10^3 km²) interpolation scheme used in this paper (see later for a full description), we are not able to resolve strain rates generated by small fault systems and any shallow sub-surface processes (< 5 – 10 km depth). The GPS strain rate field has then very much to do with lithosphere deformation and less with crust structure. The agreement between stress and strain rate tensors principal components orientations would indicate that crustal and lithosphere deformation are consistent. Two things could mask this agreement: existing fault systems and post-seismic activity. Inherited fault systems can drive the orientation of rupture along fault, orientation that may not necessarily consistent with the stress inferred of borehole breakouts.

The GPS velocity field, results of campaigns carried out over the last 2 decades. We expect the surface velocities to be representative of the interseismic deformation field plus a component of postseismic deformation. Regarding postseismic activity, thanks to studies carried out on the postseismic deformation period that followed the 2004 M_w 6 Parkfield⁹⁰ and the 2009 M_w 6.3 LAquila⁹¹ earthquakes, we know that the postseismic deformation period that follows a M_w 6.0 earthquake does not last for more than 15 months. In consequence, as the last $M_w \sim 6.0$ event in Switzerland occurred in Sierre in 1846, we assume the surface velocity field observed today is not disturbed by large scale postseismic deformation. We expect then that the velocity field observed today is representative of a period that could be longer than the time interval between the oldest and the most recent campaigns.

Geodetic data. We use the GPS surface velocity field (CHTRFv10) resulting of the processing of GPS campaigns (Table 2) and continuous GPS network data by SWISSTOPO teams^{58,69,92}. Data collected in Switzerland have been processed using sites located in Europe (GRAZ, PFA2, PFAN, WETT and ZIM2) allowing a more stable estimation of troposphere state and of the orbits parameters. Formal uncertainties on velocities ($< 10^{-5}$ m/yr) tells us that the velocity field's estimation is robust but do not reflect well the day to day repeatabilities (~ 3 mm) usually observed on time-series of permanent sites; even troposphere conditions are well constrained⁹³. For the rest of the study, and in the light of campaign characteristics (first, last epoch), we assume that uncertainties on horizontal velocities components are of 0.1 mm/yr.

Seismic data. The Swiss Seismological Service (SED, http://www.seismo.ethz.ch/index_EN) reports local seismic activity (locations, magnitudes and when possible moment tensors) and routinely estimates moment tensors and earthquake focal mechanisms. This effort resulted in an accurate catalogue of *P*- and *T*- axes^{81,94} made of 211 events located in Switzerland and surrounding areas for the period 1968–2013 (Fig. 2 and Table 3).

As these events represent only a fraction of the seismic moment released during the interseismic period, we supplement the catalogue of moment tensors with the earthquake catalogue ECOS-09 that enable us to map the spatial distribution of the seismic activity (Fig. 2c). The ECOS09 catalogue (<http://hitseddb.ethz.ch:8080/ecos09/>

introduction.html) is complete down to intensity V since 1878, IV since 1964 and Mw3.0 since 1976³⁷. We list in Table 3 the characteristics of each earthquake catalogue mentioned above.

B- Strain rate computation method. We completed an inversion of GPS horizontal velocities to constrain the amplitudes and directions of the horizontal strain rate components using the software SSPX version 2D⁹⁵. The strain rate field has been computed on a regular grid using a nearest-neighbour approach (node interval of 25 km and 6 neighbouring GPS sites included at each grid point in case they are within 50 km of the node). We assume that strain rates are not significant when rates computed from uncertainties on velocities are larger than rates computed using their amplitudes. In other words, at a specific location, if the strain rate computed from uncertainties on velocities is larger than the ones computed using velocity amplitudes, the strain rate at this location is set to zero. This approach, however, does not prevent to be more selective: we consider that any strain rate smaller than $2 \cdot 10^{-9}$ strain/yr (or a relative motion of 2 mm/yr over 1000 km) should not be trusted.

References

- Murray, M. H. & Segall, P. Modeling broadscale deformation in northern California and Nevada from plate motions and elastic strain accumulation. *Geophys. Res. Lett.* **28**, 4315–4318 (2001).
- Bennett, R. A., Rodi, W. & Reilinger, R. E. Global positioning system constraints on fault slip rates in southern California and northern Baja, Mexico. *J. Geophys. Res.* **101**(21), 943–921,960 (1996).
- d'Alessio, M. A., Johanson, I. A., Burgmann, R., Schmidt, D. A. & Murray, M. H. Slicing up the San Francisco Bay Area: block kinematics and fault slip rates from GPS-derived surface velocities. *J Geophys Res-Sol Ea* **110**, B06403 Artn b06403 (2005).
- Qizhi, C. *et al.* A deforming block model for the present-day tectonics of Tibet. *J Geophys Res* **109**, 16–16, <https://doi.org/10.1029/2002jb002151> (2004).
- Apel, E. V. *et al.* Independent active microplate tectonics of northeast Asia from GPS velocities and block modeling. *Geophys Res Lett* **33**, <https://doi.org/10.1029/2006gl026077> (2006).
- England, P. & McKenzie, D. A Thin Viscous Sheet Model for Continental Deformation. *Geophysical Journal of the Royal Astronomical Society* **70**, 295–321 (1982).
- Houseman, G. & England, P. Crustal Thickening Versus Lateral Expulsion in the Indian-Asian Continental Collision. *J Geophys Res-Sol Ea* **98**, 12233–12249 (1993).
- García-Castellanos, D. & Jimenez-Munt, I. Topographic evolution and climate aridification during continental collision: insights from computer simulations. *PLOS one*, 1–32, <https://doi.org/10.1371/journal.pone.0132252> (2015).
- Brodsky, E. E. Long-range triggered earthquakes that continue after the wave train passes. *Geophys Res Lett* **33** (2006).
- Brodsky, E. E. New constraints on mechanisms of remotely triggered seismicity at Long Valley Caldera. *J Geophys Res* **110**, <https://doi.org/10.1029/2004jb003211> (2005).
- Nadeau, R. M. & Dolenc, D. Nonvolcanic tremors deep beneath the San Andreas Fault. *Science* **307**, 389–389 (2005).
- Nadeau, R. M. & Guilhem, A. Nonvolcanic Tremor Evolution and the San Simeon and Parkfield, California, Earthquakes. *Science* **325**, 191–193, <https://doi.org/10.1126/science.1174155> (2009).
- Pollitz, F. F. & Sacks, I. S. Stress triggering of the 1999 Hector Mine earthquake by transient deformation following the 1992 Landers earthquake. *B Seismol Soc Am* **92**, 1487–1496 (2002).
- Parsons, T. Tectonic stressing in California modeled from GPS observations. *J Geophys Res-Sol Ea* **111**, <https://doi.org/10.1029/2005jb003946> (2006).
- Felzer, K. R. & Brodsky, E. E. Testing the stress shadow hypothesis. *J Geophys Res-Sol Ea* **110**, <https://doi.org/10.1029/2004jb003277> (2005).
- Houlié, N. & Phillips, R. J. Quaternary rupture behavior of the Karakoram Fault and its relation to the dynamics of the continental lithosphere, NW Himalaya–western Tibet. *Tectonophysics* **599**, 1–7, <https://doi.org/10.1016/j.tecto.2013.03.029> (2013).
- Toda, S. & Stein, R. S. Response of the San Andreas Fault to the 1983 Coalinga–Nuñez Earthquakes: An Application of Interaction-based Probabilities for Parkfield. *J. Geophys. Res.* **107** (2002).
- Perfettini, H. & Avouac, J. P. Stress transfer and strain rate variations during the seismic cycle. *J Geophys Res-Sol Ea* **109**, <https://doi.org/10.1029/2003jb002917> (2004).
- Freed, A. M. Earthquake triggering by static, dynamic, and postseismic stress transfer. *Annual Review of Earth and Planetary Sciences* **33**, 335–367, <https://doi.org/10.1146/annurev.earth.33.092203.122505> (2005).
- Bufe, C. G. Coulomb stress transfer and tectonic loading preceding the 2002 Denali fault earthquake. *B Seismol Soc Am* **96**, 1662–1674, <https://doi.org/10.1785/0120050007> (2006).
- Houlié, N. & Stern, T. A comparison of GPS solutions for strain and SKS fast directions: implications for modes of shear in the mantle of a plate boundary zone. *Earth Planet. Sci. Lett.* **345–348**, 117–125, <https://doi.org/10.1016/j.epsl.2012.06.029> (2012).
- Chamberlain, C. J., Houlié, N., Benthams, H. L. M. & Stern, T. A. Lithosphere–asthenosphere interactions near the San Andreas fault. *Earth Planet Sc Lett* **399**, 14–20, <https://doi.org/10.1016/j.epsl.2014.04.048> (2014).
- Hess, H. H. Seismic Anisotropy of the upper most mantle under oceans. *Nature* **204**, 629–631 (1964).
- Vinnik, L. P., Farra, V. & Romanowicz, B. Azimuthal Anisotropy in the Earth from Observations of SKS at GEOSCOPE and NARS Broad-Band Stations. *B Seismol Soc Am* **79**, 1542–1558 (1989).
- Silver, P. & Chan, W. Shear wave Splitting and Subcontinental Mantle Deformation. *J. Geophys. Res.* **96**(16), 429–416, 454 (1991).
- Trota, A. *et al.* Deformation studies at Furnas and Sete Cidades Volcanoes (Sao Miguel Island, Azores). Velocities and further investigations. *Geophys J Int* **166**, 952–956, <https://doi.org/10.1111/j.1365-246X.2006.03039.x> (2006).
- Houlié, N. & Romanowicz, B. Asymmetric deformation across the San Francisco Bay Area faults from GPS observations in Northern California. *Phys. Earth Planet. Inter.* **184**, 143–153 (2011).
- Hudnut, K. W., Bock, Y., Galetzka, J. E., Webb, F. H. & Young, W. H. In *Seismotectonics in convergent plate boundary* (eds Y. Fujinawa & A. Yoshida) 167–189 (Terra Scientific Publishing Company, 2002).
- Walters, R. J. *et al.* The 2009 LAquila earthquake (central Italy): A source mechanism and implications for seismic hazard. *Geophys Res Lett* **36**, <https://doi.org/10.1029/2009gl039337> (2009).
- Wiemer, S., Giardini, D., Faeh, D., Deichmann, N. & Sellami, S. Probabilistic seismic hazard assessment of Switzerland: best estimates and uncertainties. *Journal of Seismology* **13**, 449–478, <https://doi.org/10.1007/s10950-008-9138-7> (2009).
- Giardini, D., Woessner, J. & Danciu, L. Mapping Europe's Seismic Hazard. *Eos* **95**, <https://doi.org/10.1002/2014EO290001> (2014).
- Woessner, J. *et al.* The 2013 European Seismic Hazard Model - Key Components and Results. *Bulletin of Earthquake Engineering*, 1–44, <https://doi.org/10.1007/s10518-015-9795-1> (2015).
- Fäh, D. *et al.* The 1356 Basel earthquake: an interdisciplinary revision. *Geophys J Int* **178**, 351–374, <https://doi.org/10.1111/j.1365-246X.2009.04130.x> (2009).
- Meghraoui, M. *et al.* Active normal faulting in the upper Rhine graben and paleoseismic identification of the 1356 Basel earthquake. *Science* **293**, 2070–2073, <https://doi.org/10.1126/science.1010618> (2001).

35. Ferry, M., Meghraoui, M., Delouis, B. & Giardini, D. Evidence for Holocene palaeoseismicity along the Basel-Reinach active normal fault (Switzerland): a seismic source for the 1356 earthquake in the Upper Rhine graben. *Geophys J Int* **160**, 554–U552, <https://doi.org/10.1111/j.1365-246X.2005.02404.x> (2005).
36. Kozak, J., Cermak, V., Kozak, J. & Cermak, V. *Basel Earthquake*, 1356 (2010).
37. Fäh, D. *et al.* ECOS-09 Earthquake Catalogue of Switzerland Release 2011. Report and Database. Public catalogue. (Swiss Seismological Service ETH Zurich, Zurich, 2011).
38. Schwarz-Zanetti, G., Deichmann, N., Fäh, D., Masciadri, V. & Goll, J. The earthquake in Churwalden (CH) of September 3, 1295. *Eclogae Geologicae Helvetiae* **97**, 255–264, <https://doi.org/10.1007/s00015-004-1123-8> (2004).
39. Fäh, D. *et al.* Earthquake Catalogue Of Switzerland (ECOS) and the related macroseismic database. *Eclogae Geologicae Helvetiae* **96**, 219–236, <https://doi.org/10.1007/s00015-003-1087-0> (2003).
40. Gisler, M., Fäh, D. & Deichmann, N. The Valais earthquake of December 9, 1755. *Eclogae Geologicae Helvetiae* **97**, 411–422, <https://doi.org/10.1007/s00015-004-1130-9> (2004).
41. Fritsche, S., Faeh, D., Gisler, M. & Giardini, D. Reconstructing the damage field of the 1855 earthquake in Switzerland: historical investigations on a well-documented event. *Geophys J Int* **166**, 719–731, <https://doi.org/10.1111/j.1365-246X.2006.02994.x> (2006).
42. Kozak, J. & Vanek, J. The 1855 Visp (Switzerland) earthquake: Early attempts of earthquake intensity classification. *Studia Geophysica Et Geodaetica* **50**, 147–159, <https://doi.org/10.1007/s11200-006-0008-x> (2006).
43. Fritsche, S. & Faeh, D. The 1946 magnitude 6.1 earthquake in the Valais: site-effects as contributor to the damage. *Swiss Journal of Geosciences* **102**, 423–439, <https://doi.org/10.1007/s00015-009-1340-2> (2009).
44. Fritsche, S., Faeh, D. & Schwarz-Zanetti, G. Historical intensity VIII earthquakes along the Rhone valley (Valais, Switzerland): primary and secondary effects. *Swiss Journal of Geosciences* **105**, 1–18, <https://doi.org/10.1007/s00015-012-0095-3> (2012).
45. Fritsche, S. & Fäh, D. The 1946 magnitude 6.1 earthquake in the Valais: site-effects as contributor to the damage. *Swiss Journal of Geosciences* **102**, 423–439, <https://doi.org/10.1007/s00015-009-1340-2> (2009).
46. Wanner, E. & Grütter, M. Etude sur les répliques de tremblement de terre du Valais, de 1946 à 1950. *Bulletin de la Murithienne fascicule LX-VII*, 24–41 (1950).
47. Fäh, D. *et al.* Coupled seismogenic geohazards in Alpine regions. *Bollettino Di Geofisica Teorica Ed Applicata* **53**, 485–508, <https://doi.org/10.4430/bgta0048> (2012).
48. Fäh, D. And the COGEAR Working Group. In *14th World Conference on Earthquake Engineering* (Beijing, China, 2008).
49. Deichmann, N. *et al.* Earthquakes in Switzerland and surrounding regions during 2011. *Swiss Journal of Geosciences* **105**, 463–476, <https://doi.org/10.1007/s00015-012-0116-2> (2012).
50. Diehl, T. *et al.* Earthquakes in Switzerland and surrounding regions during 2012. *Swiss Journal of Geosciences* **106**, 543–558 (2013).
51. Deichmann, N. *et al.* Earthquakes in Switzerland and surrounding regions during 2001. *Eclogae Geologicae Helvetiae* **95**, 249–262 (2002).
52. Tesauro, M., Hollenstein, C., Egli, R., Geiger, A. & Kahle, H.-G. Analysis of central western Europe deformation using GPS and seismic data. *Journal of Geodynamics* **42**, 194–209, <https://doi.org/10.1016/j.jog.2006.08.001> (2006).
53. Ustaszewski, K. & Schmid, S. M. Latest Pliocene to recent thick-skinned tectonics at the Upper Rhine Graben – Jura Mountains junction. *Swiss J. Geosci.* **100**, 293–312 (2007).
54. Villiger, A., Geiger, A., U., M. & Brockmann, E. SWISS 4D: Estimation of the tectonic deformation field of Switzerland based on GPS measurements. *Swiss Academy of Sciences* (2011).
55. Anderson, H. & Jackson, J. Active Tectonics of the Adriatic Region. *Geophysical Journal of the Royal Astronomical Society* **91**, 937–983, <https://doi.org/10.1111/j.1365-246X.1987.tb01675.x> (1987).
56. Ward, S. N. Constraints on the seismo-tectonics of the central Mediterranean from very long baseline interferometry. *Geophys. J. Int.* **117**, 441–452 (1994).
57. Nocquet, J. M. & Calais, E. Crustal velocity field of western Europe from permanent GPS array solutions, 1996–2001. *Geophys. J. Int.* **154**, 72–88 (2003).
58. Battaglia, M., Murray, M., Serpelloni, E. & Bürgmann, R. The Adriatic region: An independent microplate within the Africa-Eurasia collision zone. *Geophys. Res. Lett.* **31**, <https://doi.org/10.1029/2004GL019723> (2004).
59. Serpelloni, E. *et al.* Kinematics of the Western Africa-Eurasia plate boundary from focal mechanisms and GPS data. *Geophys J Int.* **169**, 1180–1200, <https://doi.org/10.1111/j.1365-246X.2007.03367.x> (2007).
60. Menard, G., Molnar, P. & Platt, J. P. Budget of Crustal Shortening and Subduction of Continental-Crust in the Alps. *Tectonics* **10**, 231–244 (1991).
61. Schmid, S. M., Pfiffner, O. A., Froitzheim, N., Schonborn, G. & Kissling, E. Geophysical-geological transect and tectonic evolution of the Swiss-Italian Alps. *Tectonics* **15**, 1036–1064, <https://doi.org/10.1029/96tc00433> (1996).
62. Lyon-Caen, H. & Molnar, P. Constraints on the deep structure and dynamic processes beneath the Alps and adjacent regions from an analysis of gravity anomalies. *Geophys. J. Int.* **99**, 19–32 (1989).
63. Barruol, G., Bonnín, M., Pedersen, H., Bokelmann, G. H. R. & Tiberi, C. Belt-parallel mantle flow beneath a halted continental collision: The Western Alps. *Earth Planet Sc Lett* **302**, 429–438, <https://doi.org/10.1016/j.epsl.2010.12.040> (2011).
64. Champagnac, J. D., Molnar, P., Anderson, R. S., Sue, C. & Delacou, B. Quaternary erosion-induced isostatic rebound in the western Alps. *Geology* **35**, 195–198, <https://doi.org/10.1130/g23053a.1> (2007).
65. Jeanrichard, F. Contributions à l'étude du mouvement vertical des Alpes. *Boll. di Geodesia e Scienze Affini* **31**, 17–40 (1972).
66. Gubler, E., Kahle, H. G., Klingele, E., Mueller, S. & Olivier, R. Recent Crustal Movements in Switzerland and Their Geophysical Interpretation. *Tectonophysics* **71**, 125, [https://doi.org/10.1016/0040-1951\(81\)90054-8](https://doi.org/10.1016/0040-1951(81)90054-8) (1981).
67. Kahle, H. G. *et al.* In *Deep Structure of the Swiss Alps* (eds O.A. Pfiffner *et al.*) 25–259 (Birkhäuser, 1997).
68. Brockmann, E. *et al.* In *International Association of Geodesy* (ed S. Kenyon *et al.*) (Springer-Verlag Berlin Heidelberg).
69. Brockmann, E. & Schlatter, A. In *EUREF 2011 conference, May 25–28, 2011*.
70. Schlatter, A., Schneider, D., Geiger, A. & Kahle, H. G. Recent vertical movements from precise levelling in the vicinity of the city of Basel, Switzerland. *International Journal of Earth Sciences* **94**, 507–514, <https://doi.org/10.1007/s00531-004-0449-9> (2005).
71. Fuhrmann, T., Westerhaus, M., Zippelt, K. & Heck, B. Vertical displacement rates in the Upper Rhine Graben area derived from precise leveling. *J Geod.* **88** (2014).
72. Madritsch, H. *et al.* Late Quaternary folding in the Jura Mountains: evidence from syn-erosional deformation of fluvial meanders. **22**, 154 (2010).
73. Schlunegger, F. & Kissling, E. Slab rollback orogeny in the Alps and evolution of the Swiss Molasse basin. *Nature Communications* **6**, 8605, <https://doi.org/10.1038/ncomms9605> (2015).
74. Cenni, N. *et al.* Present vertical movements in central and northern Italy from GPS data: possible role of natural and anthropic causes. *Jour. Geodynamics* (2013).
75. Sue, C. & Tricart, P. Neogene to ongoing normal faulting in the inner western Alps: A major evolution of the late alpine tectonics. *Tectonics* **22**, <https://doi.org/10.1029/2002tc001426> (2003).
76. Delacou, B., Sue, C., Champagnac, J.-D. & Burkhard, M. In *Deformation Mechanisms, Rheology and Tectonics: From Minerals to the Lithosphere* Vol. 243 *Geological Society Special Publication* (eds D. Gapais, J. P. Brun, & P. R. Cobbold) 295–310 (2005).
77. Villiger, A. *Improvement of the Kinematic Model of Switzerland (Swiss 4D II)* PhD thesis, ETH (2014).
78. Limpach, P., Villiger, A. & Geiger, A. Swiss National Report on the GEODETIC ACTIVITIES in the years 2011 to 2015 (IUGG, Prague, 2015).

79. Mock, S. & Herwegh, M. Tectonics of the central Swiss Molasse Basin: Post-Miocene transition to incipient thick-skinned tectonics? *Tectonics* **36**, 1699–1723, <https://doi.org/10.1002/2017TC004584> (2017).
80. Serpelloni, E., Anzidei, M., Baldi, P., Casula, G. & Galvani, A. Crustal velocity and strain-rate fields in Italy and surrounding regions: new results from the analysis of permanent and non-permanent GPS networks. *Geoph. J. Int.* **161**, 861–880 (2005).
81. Kastrup, U. Stress field variations in the Swiss Alps and the northern Alpine foreland derived from inversion of fault plane solutions. *J. Geophys. Res.* **109**, <https://doi.org/10.1029/2003jb002550> (2004).
82. Scheidegger, A. E. The tectonic stress and tectonic motion direction in Europe and Western Asia as calculated from earthquake fault plane solutions. *Bull. Seis. Soc. Am.* **54**, 1519–1528 (1964).
83. Shirokova, E. I. General features in the orientation of principal stresses in earthquake foci in the Mediterranean-Asian seismic belt. *Physics of the Solid Earth*, 12–22 (1967).
84. Hardebeck, J. L. & Michael, A. J. Stress orientations at intermediate angles to the San Andreas Fault, California. *J. Geophys. Res.* **109**, <https://doi.org/10.1029/2004jb003239> (2004).
85. McKenzie, D. The relationship between fault plane solutions for earthquakes and the directions of the principal stresses. *B. Seismol. Soc. Am.* **59**, 591–601 (1969).
86. Teng, L. S. Extensional collapse of the northern Taiwan mountain belt. *Geology* **24**, 949–952, [https://doi.org/10.1130/0091-7613\(1996\)024<0949:ecotnt>2.3.co;2](https://doi.org/10.1130/0091-7613(1996)024<0949:ecotnt>2.3.co;2) (1996).
87. Platt, J. P. & Vissers, R. L. M. Extensional collapse of thickened continental lithosphere – a working hypothesis for the Alboran sea and Gibraltar arc. *Geology* **17**, 540–543, [https://doi.org/10.1130/0091-7613\(1989\)017<0540:ecotcl>2.3.co;2](https://doi.org/10.1130/0091-7613(1989)017<0540:ecotcl>2.3.co;2) (1989).
88. Walcott, D. The kinematics of the plate boundary zone through New Zealand: a comparison of short- and long-term deformations. *Geophys. J. Astr. Soc.* **79**, 613–633 (1984).
89. Freed, A. M., Ali, S. T. & Bürgmann, R. Evolution of stress in Southern California for the past 200 years from coseismic, postseismic and interseismic stress changes. *Geophys. J. Int.* **169**, 1164–1179, <https://doi.org/10.1111/j.1365-246X.2007.03391.x> (2007).
90. Savage, J. C. & Langbein, J. Postearthquake relaxation after the 2004 M6 Parkfield, California, earthquake and rate-and-state friction. *J. Geophys. Res.* **113**, <https://doi.org/10.1029/2008JB005723> (2008).
91. Devoti, R. *et al.* The coseismic and postseismic deformation of the LAquila, 2009 earthquake from repeated GPS measurements. *Ital. J. Geosci.* **131**, 348–358, <https://doi.org/10.3301/IJG.2012.15> (2012).
92. Brockmann, E., Marti, U., Schlatter, A. & Schneider, D. CHCGN activities in Switzerland Activities for a Swiss Combined Geodetic Network. (SWISS TOPO Bern, 2003).
93. Houlié, N., Funning, G. & Bürgmann, R. Use of a GPS-derived troposphere model to improve InSAR deformation estimates in the San Gabriel Valley, California. *Trans. Geosc. Rem. Sensing* **54**, 5365–5374, <https://doi.org/10.1109/TGRS.2016.2561971> (2016).
94. Marschall, I., Deichmann, N. & Marone, F. Earthquake focal mechanisms and stress orientations in the eastern Swiss Alps. *Swiss J. Geosci.* **106**, 1–12, <https://doi.org/10.1007/s00015-013-0129-5> (2013).
95. Cardozo, N. & Allmendinger, R. SSPX: A program to compute strain from displacement/velocity data. *Computers and Geosciences* **35**, 1343–1357 (2009).
96. Serpelloni, E., Faccenna, C., Spada, G., Dong, D. & Williams, S. D. P. Vertical GPS ground motion rates in the Euro-Mediterranean region: New evidence of velocity gradients at different spatial scales along the Nubia-Eurasia plate boundary. *J. Geophys. Res. Solid Earth* **118**, 6003–6024, <https://doi.org/10.1002/2013JB010102> (2013).
97. Wagner, M., Kissling, E. & Husen, S. Combining controlled-source seismology and local earthquake tomography to derive a 3-D crustal model of the western Alpine region. *Geophys. J. Int.* **191**, 789–802, <https://doi.org/10.1111/j.1365-246X.2012.05655.x> (2012).
98. Spada, M., Bianchi, I., Kissling, E., Agostinetti, N. P. & Wiemer, S. Combining controlled-source seismology and receiver function information to derive 3-D Moho topography for Italy. *Geophys. J. Int.* **194**, 1050–1068, <https://doi.org/10.1093/gji/ggt148> (2013).
99. Wessel, P., Smith, W. H. F., Scharroo, R., Luis, J. F. & Wobbe, F. Generic Mapping Tools: Improved version released. *EOS Trans. AGU* **94**, (409–410) (2013).
100. Delacou, B., Sue, C., Champagnac, J. D. & Burkhard, M. Present-day geodynamics in the bend of the western and central Alps as constrained by earthquake analysis. *Geophys. J. Int.* **158**, 753–774, <https://doi.org/10.1111/j.1365-246X.2004.02320.x> (2004).
101. International Seismological Centre, On-line Bulletin. (International Seismological Centre, Thatcham, United Kingdom, 2015).
102. Fry, B., Deschamps, F., Kissling, E., Stehly, L. & Giardini, D. Layered azimuthal anisotropy of Rayleigh wave phase velocities in the European Alpine lithosphere inferred from ambient noise. *Earth Planet Sc Lett* **297**, 95–102, <https://doi.org/10.1016/j.epsl.2010.06.008> (2010).
103. Reinecker, J., Tingay, M., Muller, B. & Heidbach, O. Present-day stress orientation in the Molasse Basin. *Tectonophysics* **482**, 129–138, <https://doi.org/10.1016/j.tecto.2009.07.021> (2010).
104. Singer, J., Diehl, T., Husen, S., Kissling, E. & Duretz, T. Alpine lithosphere slab roll back causing lower crustal seismicity in northern foreland. *Earth & Planet. Sc. Lett.* **397**, 42–56 (2014).
105. Brockmann, E., Schlatter, A., Marti, U. & Schneider, D. CHCGN activities in Switzerland, Activities for a Swiss Combined Geodetic Network. (Swiss topo, 2004).
106. Deichmann, N. *et al.* Earthquakes in Switzerland and surrounding regions during 1997. *Eclogae Geologicae Helvetiae* **91**, 237–246 (1998).
107. Marshall, S. T., Funning, G. J. & Owen, S. E. Fault slip rates and interseismic deformation in the western Transverse Ranges, California. *J. Geophys. Res.-Sol Ea* **118**, 4511–4534, <https://doi.org/10.1002/jgrb.50312> (2013).

Acknowledgements

We thank Pr. E. Kissling, Pr. S. Schmid, Dr. A. Villiger, Dr. V. Picotti and the writing club group of SEG for their contributions in improving the manuscript. We also thank Pr. Dr. Niu and Pr. Dr. Schlunegger plus two anonymous reviewers. This work could not have been possible without the support of the ARC1/ARC2 team of the University of Leeds, UK.

Author Contributions

N.H. initial idea; N.H. and J.W. completed the figures design; N.H., J.W., D.G., and M.R. wrote the text.

Additional Information

Supplementary information accompanies this paper at <https://doi.org/10.1038/s41598-018-20253-z>.

Competing Interests: The authors declare that they have no competing interests.

Publisher's note: Springer Nature remains neutral with regard to jurisdictional claims in published maps and institutional affiliations.



Open Access This article is licensed under a Creative Commons Attribution 4.0 International License, which permits use, sharing, adaptation, distribution and reproduction in any medium or format, as long as you give appropriate credit to the original author(s) and the source, provide a link to the Creative Commons license, and indicate if changes were made. The images or other third party material in this article are included in the article's Creative Commons license, unless indicated otherwise in a credit line to the material. If material is not included in the article's Creative Commons license and your intended use is not permitted by statutory regulation or exceeds the permitted use, you will need to obtain permission directly from the copyright holder. To view a copy of this license, visit <http://creativecommons.org/licenses/by/4.0/>.

© The Author(s) 2018